# ProtoTSNet: Interpretable Multivariate Time Series Classification With Prototypical Parts

Bartłomiej Małkus¹ — Szymon Bobek² — Grzegorz J. Nalepa²

Doctoral School of Exact and Natural Sciences
Jagiellonian University
Cracow, Poland
bartlomiej.malkus@doctoral.uj.edu.pl

Faculty of Physics, Astronomy and Applied Computer Science, Institute of Applied Computer Science, and Jagiellonian Human-Centered AI Lab Jagiellonian University Cracow, Poland

#### Abstract

{szymon.bobek, grzegorz.j.nalepa}@uj.edu.pl

Time series data is one of the most popular data modalities in critical domains such as industry and medicine. The demand for algorithms that not only exhibit high accuracy but also offer interpretability is crucial in such fields, as decisions made there bear significant consequences. In this paper, we present ProtoTSNet, a novel approach to interpretable classification of multivariate time series data, through substantial enhancements to the ProtoPNet architecture. Our method is tailored to overcome the unique challenges of time series analysis, including capturing dynamic patterns and handling varying feature significance. Central to our innovation is a modified convolutional encoder utilizing group convolutions, pretrainable as part of an autoencoder and designed to preserve and quantify feature importance. We evaluated our model on 30 multivariate time series datasets from the UEA archive, comparing our approach with existing explainable methods as well as non-explainable baselines. Through comprehensive evaluation and ablation studies, we demonstrate that our approach achieves the best performance among ante-hoc explainable methods while maintaining competitive performance with non-explainable and post-hoc explainable approaches, providing interpretable results accessible to domain experts.

# 1 Introduction

In recent years, the field of *time series classification* (TSC) has received significant attention in diverse domains, including healthcare [22], finance [36], and industry [23]. While recent research in this field has focused primarily on improving model accuracy, aspects such as explainability and computational

efficiency have often been overlooked. Although state-of-the-art models achieve impressive performance on benchmark datasets, they remain largely opaque and frequently face scalability challenges [4, 28].

This opacity stands in stark contrast to emerging requirements for AI transparency and explainability, initially outlined by [7] and subsequently mandated through regulatory frameworks such as GDPR [16] and the more recent AI Act [17]. Our work addresses this gap by developing an explainable TSC approach while maintaining competitive performance and scalability.

Explainable methods in machine learning are commonly categorized into post hoc and ante hoc approaches. Post hoc methods provide retrospective explanations of a model's decisions while the model itself remains a black box, an approach particularly common in neural networks [30]. However, these explanations may be inaccurate or lead to misconceptions about the model's operations [31]. In contrast, ante hoc architectures incorporate explainability directly into the model's design, offering a more transparent and immediate understanding of the decision-making processes. Among these, prototype-based methods have gained significant attention, with ProtoPNet [6] being a notable example. These methods explain decisions through a set of learned prototypes, providing interpretable insights by highlighting key representative patterns that influence predictions.

Following recent surveys in the field of explainable time series classification [38], two significant observations can be made. First, a large part of existing studies focus on univariate time series. Multivariate data presents additional complexities, including the potential inter-feature dependencies and feature redundancy. Secondly, a large part of the studies do not provide a way to reproduce the results, which is imposing what is becoming known as the replication crisis [21]. In the context of explainability, we strive for transparency, and the ability to replicate findings is a crucial component of transparent research.

Our work introduces a neural network architecture for Interpretable Time Series Classification with Prototypical Parts (ProtoTSNet) that leverages the principles of the ProtoPNet architecture and spans to univariate and multivariate time-series datasets. Although there have been similar endeavors to apply ProtoPNet's architecture or its foundational ideas [25] to time series analysis [15, 29], they are limited to univariate series, their effectiveness is not tested on a wider range of problems, and/or source code is unavailable. We present a unique take on this problem, as our architecture differs from the mentioned works by introducing a custom encoder and training process modified to capture the prototypical parts in time-series. The general idea behind ProtoTSNet is shown in Figure 1.

Notably, our work addresses a relatively unexplored area in the literature by offering an ante hoc explainable approach for multivariate time series data. Moreover, in the process of comparison with the selected methods in the literature, we rerun experiments to verify their ability to achieve the reported results. Based on the benchmarks we conducted on publicly available datasets, our method outperforms state-of-the-art explainable methods. Recognizing the importance of reproducibility, we ensure the accessibility of our method by publishing its source code<sup>1</sup>.

The remainder of the paper is organized as follows. In Section 2 we present

<sup>&</sup>lt;sup>1</sup>The code is published at https://github.com/bmalkus/ProtoTSNet

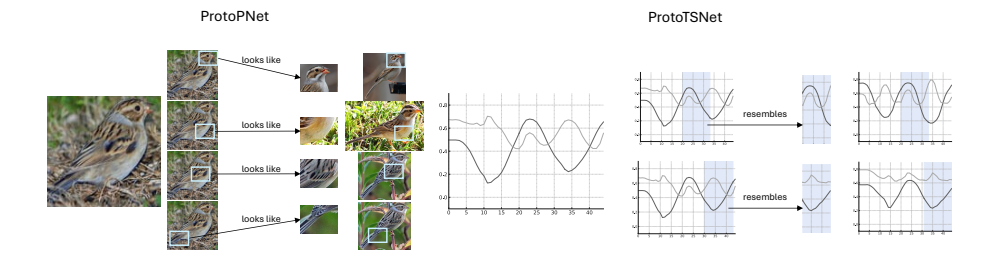


Figure 1: The general idea of how ProtoPNet and ProtoTSNet classify instances. In the case of ProtoPNet, it can be read as "this patch from the test image looks like that prototypical part from the training set." In the case of ProtoTSNet, it is "this subsequence from the test instance resembles that prototypical part from the training set." The ProtoPNet part of the image is sourced from its authors [6].

an overview of the state-of-the-art methods in the area of explainable AI for time series. In Section 3 we state the problem and introduce the mathematical basis to describe our approach in detail in Section 4. We describe the evaluation and discuss the results in Section 5. We conclude our paper in Section 6.

# 2 Related Work

In this section, we review recent advances in explainable time series classification, focusing on multivariate time series. The existing explainable methods can be categorized into ante-hoc methods, which incorporate interpretability directly into their architecture, and post-hoc methods, which apply explanatory techniques after model training.

#### 2.1 Post-hoc Explainable Methods

Post-hoc methods include model-agnostic approaches such as SHAP [27] and LIME [33], and model-specific techniques like Grad-CAM [35]. In time series classification, Grad-CAM has been adapted to identify both relevant temporal segments and significant features, though this requires a specific architectural design.

MTEX-CNN [1], designed for multivariate time series, employs a two-stage architecture. The first stage processes input data of size  $(T \times D)$ , where T denotes the temporal dimension and D the number of features, using two-dimensional convolutions with  $(k \times 1)$  kernels, independently processing each feature while retaining feature count and increasing channels. The second stage applies one-dimensional convolutions with  $(k \times D)$  kernels temporally, followed by dense layers for classification. Grad-CAM is integrated with both stages to highlight feature contributions and temporal patterns. The method's reproducibility is limited, as no implementation was provided.

XCM [13], another multivariate approach, extracts temporal and feature relevance in parallel rather than sequentially. It processes  $(T \times D)$  input through

two modules: one using  $(k \times 1)$  kernels for feature processing and another applying one-dimensional convolutions with  $(k \times D)$  kernels temporally. The outputs are combined and processed through additional convolutions and dense layers. The authors provided source code for both XCM and MTEX-CNN implementations, although our experiments did not replicate their reported performance.

LITEMVTime [20] is a post-hoc explainable method that applies Class Activation Maps (CAMs) to provide interpretability for multivariate time series classification. Built on the LITE architecture, which uses depthwise separable convolutions and boosting techniques, LITEMVTime generates temporal importance scores indicating which time stamps contribute the most to classification decisions. The method has been demonstrated on human rehabilitation exercise evaluation, showing both competitive performance and explainability.

A more recent alternative to Grad-CAM, Dimension-wise Class Activation Mapping (dCAM) [3], specifically designed for multivariate time series, examines feature contributions directly through gradient analysis. Unlike Grad-CAM's focus on feature maps, dCAM generates temporal importance scores for each dimension, providing insights into feature interactions and temporal evolution.

# 2.2 Ante-hoc Explainable Methods

Ante-hoc methods include traditional interpretable models like decision trees or rule-based systems and modern neural network-based solutions. PETSC [14] transforms time series using Symbolic Aggregate Approximation (SAX) [26] to identify frequent sequential patterns of varying lengths. Although it supports both univariate and multivariate data, its explainability is limited to univariate cases. The method includes publicly available source code and performs well compared to other interpretable models.

LAXCAT [19], designed for multivariate time series, combines convolutional processing with dual attention mechanisms: variable attention for key features and temporal attention for critical intervals. While providing instance-level explanations, the lack of source code limits reproducibility.

MrSEQL [24], limited to univariate data, combines SAX and Symbolic Fourier Approximation (SFA) representations, using an extended Sequence Learner to mine discriminative patterns. The authors provide the source code and results of the evaluation on the UCR Time Series Archive.

The r-STSF [5] method calculates aggregate statistics for subseries across multiple representations (frequency domain, derivative, and autoregressive), constructing a forest of randomized binary trees. While efficient and interpretable, it currently handles only univariate data. The method includes complete source code implementation.

#### 2.3 Prototype-based time series classification

While prototype-based methods could be categorized under both ante-hoc and post-hoc approaches, we present them separately due to their particular relevance to our proposed method. These methods learn representative patterns from training data - either complete sequences or discriminative fragments - that serve as references for classification decisions. While they can provide interpretable insights through prototype comparison, the explainability aspect is not always explored in existing approaches. Although extensively studied in

computer vision [32, 34], applying prototype-based methods to time series data presents unique challenges, particularly in handling temporal dependencies and varying sequence lengths.

ProtoFac [8] is a post-hoc method supporting multivariate time series. It replaces selected neural network layers with a prototype matrix through explainable factorization, constraining prototypes to realistic data segments while maintaining model fidelity. The method decomposes latent activations into interpretable prototypes and corresponding weights after model training, though lack of source code limits reproduction.

ProSeNet [29] takes an ante-hoc approach for univariate data, incorporating interpretability directly by learning whole-instance prototypes from RNN latent space during training. The method optimizes for simplicity, diversity, and sparsity, and allows domain experts to refine prototypes without altering the model structure, but no implementation was provided.

Gee et al. [15] present another ante-hoc approach focused exclusively on univariate time series. Their autoencoder-prototype architecture learns prototypes directly from the latent space during training, with a diversity penalty ensuring representative coverage of the data distribution. The method lacks publicly available implementation.

DPSN [37] is an ante-hoc method that combines "representative shapelets" (whole instances as prototypes) with "discriminative shapelets" (differentiating sub-sequences) for few-shot learning. The method uses SFA features and metric learning. The source code is provided, but the method remains limited to univariate data.

Table 1: Comparison of state of the art methods from the literature with ours.

Method	Multivariate	Ante-hoc explainable	Source code provided
MTEX-CNN [1]	<b>√</b>		1
XCM [13]	✓		✓
LITEMVTime	./		
[20]	<b>v</b>		•
PETSC [14]	✓	2	✓
LAXCAT [19]	✓	✓	
MrSEQL [24]		✓	✓
r-STSF [5]		✓	✓
ProtoFac [8]	✓		
ProSeNet [29]		✓	
- [15]		✓	
DPSN [37]		✓	✓
${\bf ProtoTSNet}$	✓	$\checkmark$	✓

# 3 Preliminaries

In this section, we outline the core objectives and challenges that our research addresses in the context of explainable time series classification. We define the problem of multivariate time series classification, discuss feature importance in time series analysis, and then discuss the prototype term.

#### 3.1 Multivariate Time Series Classification

A multivariate time series X is represented as a matrix  $X \in \mathbb{R}^{d \times T}$ , where d denotes the number of dimensions (features) and T denotes the length of the time series. Each feature (dimension) of X can be represented as  $X_i$ , where  $i = 1, 2, \ldots, d$ , and each  $X_i$  is a sequence of observations over time  $t = 1, 2, \ldots, T$ .

The classification task involves the construction of a function  $f: \mathbb{R}^{d \times T} \mapsto \{1, 2, \dots, C\}$  that maps a multivariate time series X to a class label  $y \in \{1, 2, \dots, C\}$ , where C is the number of classes. This function f is learned from a training set  $\{(X^{(1)}, y^{(1)}), (X^{(2)}, y^{(2)}), \dots, (X^{(n)}, y^{(n)})\}$  consisting of n pairs of multivariate time series and their corresponding class labels. The challenge in MTSC is to effectively capture both the temporal dynamics within each feature  $X_i$  and the interactions between different features to make accurate predictions about the class label y.

### 3.2 Feature Importance in Time Series Analysis

Understanding the importance of features in time series classification is essential both for model interpretation and effectiveness. In this context, feature importance refers to the relative significance of each feature (or dimension) in contributing to the model's predictive performance. Identifying key features helps in uncovering the underlying patterns and relationships that drive the prediction outcomes.

Mathematically, let us denote the feature importance vector as  $I \in \mathbb{R}^d$ , where each element  $I_i$  represents the importance of the *i*-th feature in the classification model. The aim is to evaluate I in a way that highlights the features that have a significant impact on the model's decisions.

# 3.3 Prototypes in Time Series Analysis

The term "prototype" in time series classification has varied interpretations across the literature. Some studies consider prototypes as representative full-length time series [15, 39], while others treat them as subsequences, either proper, maintaining temporal order [8], or improper, capturing similar patterns across different series [29, 37].

In our work, we define prototypical parts as proper subsequences of multivariate time series. Formally, for an input series  $X \in \mathbb{R}^{d \times T}$ , a prototypical part  $P = X_{*,[t_s:t_e]}$  spans all features (\*) over a temporal segment  $[t_s:t_e]$ , where  $1 \leqslant t_s < t_e \leqslant T$  and  $L = t_e - t_s + 1$ . These prototypes exist in both the input space (P) and the encoded space  $(P_l \in \mathbb{R}^{l \times L})$ , with mappings between them. Using proper subsequences, our approach introduces higher granularity and flexibility into the classification process, improving both interpretability and performance by focusing on the most informative segments of the data through prototype identification and feature importance calculation.

# 4 Prototypical Parts

In this section, we introduce our proposed architecture designed for multivariate time series. We discuss the general principle of operation, the proposed encoder architecture, and the calculation of the feature importance.

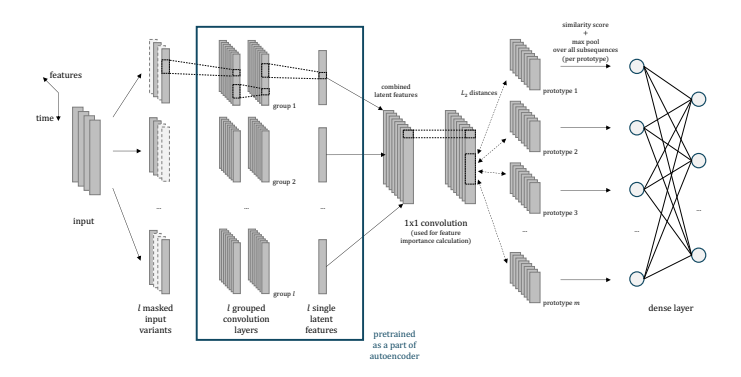


Figure 2: Model Architecture. The input multivariate time series is processed through l binary masks, each preserving a different subset of features controlled by reception parameter r. These masked variants are fed into a grouped convolution encoder (l groups), where each group processes a distinct feature subset independently, producing a single latent feature per group. The encoder outputs are mixed through a  $1 \times 1$  convolution layer, whose weights enable feature importance calculation. The prototype layer then computes  $L_2$  distances between latent subsequences and learned prototypes, applying max pooling over all subsequences to obtain similarity scores per prototype. Finally, these similarity scores are processed by a dense layer to produce class predictions.

#### 4.1 Model Architecture

Our approach draws inspiration from the architecture of ProtoPNet [6], but introduces several key modifications, specifically designed to handle multivariate time series data. At its core, the architecture implements a feature masking mechanism combined with grouped convolutions, enabling both effective feature representation learning and interpretability through feature importance calculations. The complete architecture is illustrated in Figure 2.

#### 4.1.1 Input Processing and Feature Masking

The first distinctive element of our architecture is the introduction of a feature masking mechanism. Given an input multivariate time series with d features, we generate l binary masks, where l represents the number of encoder groups (typically l=32 in our experiments). Each mask has a length equal to the number of input features (d).

For the *i*-th encoder group, each mask element  $\delta_{im} \in \{0,1\}$  determines whether the *m*-th input feature is retained (1) or masked out (0). The proportion of retained features is controlled by a parameter  $r \in (0,1)$ , called the reception parameter, which determines how many features each group receives. Specifically, each mask retains exactly  $|r \cdot d|$  randomly selected features.

For example, with d=10 input features, l=4 groups, and r=0.5, we generate 4 binary masks, each retaining 5 randomly selected features from the original 10. This process yields l variants of the input time series, each preserving a different subset of features, where each subset contains exactly  $\lfloor r \cdot d \rfloor$  features.

The parameters l and r serve complementary roles: l determines the number

of parallel processing groups (and consequently the dimensionality of the latent prototype space), while r controls the sparsity of features within each group, affecting both the computational efficiency and the quality of the calculation of features importance.

The goal of this masking process is to prevent the mixing of information between dimensions that carry significant information (prototypical parts) and those that do not (e.g., dimensions considered as noise). In the case of image modalities, all channels (e.g., RGBA) are typically considered important for building a prototype. Conversely, in time series data, the channels (or dimensions) might be less tightly connected. As a result, separating these dimensions during the prototype selection process plays a crucial role in ensuring the effectiveness of the approach.

#### 4.1.2 Grouped Convolution Encoder

The masked input variants are processed through a convolutional encoder that employs group convolution with l groups. Given an input time series  $X \in \mathbb{R}^{d \times T}$ , after feature masking, we obtain l masked variants, each of shape  $\mathbb{R}^{d \times T}$  (with  $(1-r) \cdot d$  features zeroed out).

The grouped convolution encoder processes these variants with the following shape transformations:

- Input: l masked variants of shape [batch\_size, d, T]
- Grouped Convolution Layers: Each group processes its corresponding masked input independently. Each group produces a single latent feature of shape [batch\_size, 1, T].
- Single Latent Features: Since each group outputs exactly one feature, we refer to these as "single latent features." The combined outputs (latent features) from all l groups have the shape [batch\_size, l, T].

Unlike standard convolution layers where all inputs are connected to all outputs, group convolution restricts connections to occur only within designated groups. By setting the number of groups to l in every group convolution layer, each masked input variant is processed by an independent group, effectively serving as a mini-encoder, preventing information mixing between different feature subsets.

#### 4.1.3 Feature Mixing and Prototype Space

The separated feature representations from the grouped encoder (shape  $[batch\_size, l, T]$ ) are subsequently processed through a  $1 \times 1$  convolution layer. This layer maintains the shape.

The primary purpose of this layer is to perform a controlled mixing of information from different feature subsets, enabling the calculation of feature importance through analysis of the mixing weights (detailed in Section 4.2 below). The output of this layer forms the *prototype latent space* where the prototype distance calculations are performed.

The final shape entering the prototype layer is  $[batch\_size, l, T]$ , where subsequences of length L are extracted for prototype matching.

#### 4.1.4 Prototype Layer and Classification

The prototype layer computes similarities between learned prototypes and subsequences in the latent space. Given the latent representation  $Z \in \mathbb{R}^{l \times T}$  from the  $1 \times 1$  convolution layer (Section 4.1.3), we extract all possible subsequences of length L along the temporal dimension.

Specifically, for each prototype  $P_l^{(j)} \in \mathbb{R}^{l \times L}$  from the set of m prototypes and all subsequences  $\tilde{Z} \in \mathbb{R}^{l \times L}$  of length L in the latent series Z, the layer calculates  $L_2$  distances and transforms them into similarity scores. This transformation is formalized as:

$$sim(P_l^{(j)}, Z) = \max_{\tilde{Z} \in subseq(Z)} \log \left( \frac{\left\| \tilde{Z} - P_l^{(j)} \right\|_2^2 + 1}{\left\| \tilde{Z} - P_l^{(j)} \right\|_2^2 + \epsilon} \right)$$
 (1)

where  $\epsilon$  is a small constant that prevents division by zero, and subseq(Z) denotes the set of all subsequences of length L extracted from Z.

The layer focuses on the most significant match within the series by selecting the maximum similarity score for each prototype across all possible subsequences. This max-pooling operation ensures that each prototype activation represents the strongest match found anywhere in the input time series.

These maximum similarity scores serve as prototype activations, which are then transformed into class predictions through a dense layer performing linear combination. The dense layer learns which prototypes are the most indicative of each class, enabling the final classification decision.

Since the temporal structure is preserved in the latent space, prototypes can be directly mapped back to segments in the input space, taking into account the receptive field. This direct mapping enables a straightforward interpretation of the learned representations, allowing domain experts to understand which temporal patterns the model considers important for classification.

# 4.2 Feature Importance Calculation

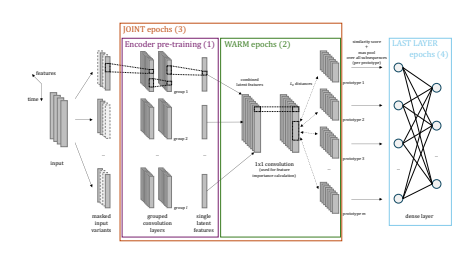
The proposed architecture enables direct calculation of feature importance by leveraging its controlled feature mixing mechanism. The key aspect of this calculation lies in the weights of the  $1 \times 1$  convolution layer that follows the grouped convolution encoder structure. To calculate the importance of a given input feature, we analyze how it influences each feature in the prototype space through the network's connectivity pattern. For the m-th input feature, its contribution is determined by two factors:

- the binary masks that control which encoders receive this feature,
- the weights in the  $1 \times 1$  convolution layer that mix the encoder outputs.

Formally, the importance  $I_m$  of the m-th input feature is calculated as:

$$I_m = \sum_{i=1}^l \left( \left\| \sum_{i=1}^l \delta_{im} w_{ij} \right\| \right) \tag{2}$$

where:



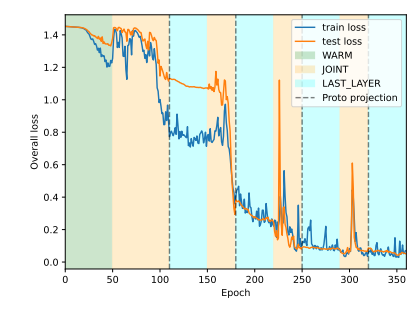


Figure 3: The training process of ProtoTSNet and its different stages mapped to the learning curve. Numbers in brackets represent order of the training stage.

- i indexes the encoder outputs (inputs to the convolution layer),
- *j* indexes the features in the prototype space (outputs of the convolution layer)
- $\delta_{im} \in 0, 1$  indicates whether the *m*-th feature is included in the *i*-th encoder's input
- $w_{ij}$  represents the weight connecting the *i*-th encoder output to the *j*-th prototype space feature

This calculation first determines the contribution of feature m to each prototype space feature j by summing the relevant pathway weights  $(\delta_{im}w_{ij})$ . The absolute values of these contributions are then summed across all prototype space features to obtain the overall importance score. This approach ensures that both positive and negative influences are captured in the final importance measure.

There are two important considerations that affect the feature importance calculations. First, the method produces global feature importance scores that characterize the overall influence of each feature across all prototypes, rather than prototype-specific importance values. Second, the reliability of these importance scores is tied to the encoder's reception parameter r. This parameter creates a trade-off: larger r values allow more features to be processed simultaneously by each encoder, potentially leading to importance score overestimation due to increased feature interaction, while smaller r values maintain feature separation but may miss some of the contextual relationships.

# 4.3 Training Process

The complete training process consists of two distinct phases: encoder pretraining and main ProtoTSNet training, as illustrated in Figure 3 and detailed in Algorithm 1.

**Phase 1: Encoder Pretraining.** We train a standard autoencoder to reconstruct the input time series using MSE loss. No prototypes are involved - the goal is to learn meaningful feature representations. After pretraining, we discard the decoder and retain only the encoder weights.

Phase 2: Main ProtoTSNet Training. We introduce the prototypes as learnable parameters and train the complete architecture. The pretrained encoder weights serve as initialization, while prototypes are randomly initialized in the latent space. The training follows a cyclical process consisting of four stages, repeated multiple times:

- 1. Warm epochs: SGD optimization applied exclusively to prototypes and the  $1 \times 1$  convolution layer weights, while encoder parameters remain frozen. This allows prototypes to adapt to the pretrained latent space.
- 2. **Joint epochs:** SGD optimization extended to include all parameters (prototypes, 1 × 1 convolution layer, and encoder). An exponential decay cyclic learning rate scheduler is employed to enhance exploration of the prototype space.
- 3. **Prototype projection:** Each prototype is projected onto the closest latent patch from the training data, ensuring that prototypes correspond to actual patterns observed in the training set. This step is crucial for maintaining the "this resembles that" interpretability property.
- 4. Last layer optimization: Only the final dense layer is optimized while all other parameters remain frozen, allowing the model to learn optimal prototype-to-class mappings.

The model's training is guided by different loss functions depending on the training stage:

Warm and Joint Epochs Loss:

$$\mathcal{L}_{main} = \mathcal{L}_{ce} + \lambda_{clst} \mathcal{L}_{clst} + \lambda_{sep} \mathcal{L}_{sep} + \lambda_{conv} \mathcal{L}_{l1\_conv}$$
 (3)

Last Layer Optimization Loss:

$$\mathcal{L}_{last} = \mathcal{L}_{ce} + \lambda_{last} \mathcal{L}_{l1\_last} \tag{4}$$

where:

- 1.  $\mathcal{L}_{ce}$  is the cross-entropy loss for classification accuracy.
- 2.  $\mathcal{L}_{clst}$  (clustering regularization) is defined as:

$$\mathcal{L}_{clst} = \frac{1}{n} \sum_{i=1}^{n} \min_{j: P_l^{(j)} \in \mathcal{P}_{y_i}} \min_{\tilde{Z} \in \text{subseq}(Z_i)} \|\tilde{Z} - P_l^{(j)}\|_2^2$$
 (5)

which encourages each training series to have at least one latent subsequence close to a prototype of its class.

3.  $\mathcal{L}_{sep}$  (separation regularization) is defined as:

$$\mathcal{L}_{sep} = -\frac{1}{n} \sum_{i=1}^{n} \min_{j:P_{l}^{(j)} \notin \mathcal{P}_{y_{i}}} \min_{\tilde{Z} \in \text{subseq}(Z_{i})} \|\tilde{Z} - P_{l}^{(j)}\|_{2}^{2}$$
 (6)

which encourages latent subsequences to remain distant from prototypes of other classes.

#### **Algorithm 1** Simplified flow of the training process

#### Require:

```
E_P := number of pretraining epochs
   E_W := number \ of \ warm \ epochs
   E_L := last\ layer\ optimization\ epochs
   I_P := number of joint epochs between pushes
 1: for epoch := 1 to E_P do
       Pretrain encoder on training data (as part of autoencoder)
3: end for
 4: for epoch := 1 to E_W do
       // Warm epoch
       Train prototypes layer only
 6:
7: end for
   while end condition not met do
       for epoch := 1 to I_P do
9:
10:
           // Joint epoch
           Train prototypes layer along with encoder
11:
       end for
12:
       // Push
13:
       Project each prototype onto closest latent patch in training data
14:
15:
       for epoch := 1 to E_L do
           // Last layer epoch
16:
           Train only the last layer
17:
       end for
18:
19: end while
```

- 4.  $\mathcal{L}_{l1\_conv}$  applies L1 sparsity regularization to the 1 × 1 convolution layer weights, helping identify important features.
- 5.  $\mathcal{L}_{l1\_last}$  applies L1 regularization to negative weights in the last layer. Since the last layer connects prototype activations to class predictions, negative weights represent "negative evidence" (e.g., "this is class 1 because it does NOT resemble prototype of class 2"). By penalizing negative weights, we encourage the model to rely on positive prototype evidence for classification, improving interpretability.

Here,  $\mathcal{P}_{y_i}$  denotes the set of prototypes belonging to class  $y_i$ ,  $Z_i$  is the latent representation of the *i*-th training series, and subseq $(Z_i)$  represents all subsequences of length L extracted from  $Z_i$ . The clustering and separation terms shape the latent space into a semantically meaningful structure, while the last layer optimization ensures sparsity in cross-class prototype connections, avoiding negative reasoning patterns.

#### 5 Experimental evaluation

In this section, we describe experimental evaluation of ProtoTSNet. We start with an experiment conducted on a synthetic dataset designed to test our model's capability in identifying regions of importance within time series data and to calculate feature importance. We then move on to the suite of experiments conducted on the UEA datasets archive<sup>2</sup>. This evaluation allows us to compare our model against state of the art models in the field of time series classification.

#### 5.1 Synthetic Dataset

Our synthetic dataset consists of three features, of which two are significant for class distinction and one is not. It contains four classes, each marked by distinct saw and rectangular patterns in significant features. A small amount of white noise is introduced into the series. Significant parts are limited to the initial 40 time steps, the subsequent 60 are randomized and independent from the classes.

The model was trained for four cycles of (joint epochs  $\rightarrow$  prototype projection  $\rightarrow$  last layer optimization), with reception of 0.75, prototype length of 20, and one prototype per class. The model achieved 100% classification accuracy as expected for this simple dataset. Figure 4 presents the learned prototypes and calculated feature importance score.

The prototypes have correctly captured the significant fragments of the input across all classes, demonstrating the model's capability to identify key temporal patterns. The coverage of significant parts varies between classes - for example, in class 3, the prototype includes a substantial portion of insignificant area. This stems from our model's design, where prototype activation is driven by similarity measures, allowing partial matches with class-specific segments to cause significant activation. In real-world scenarios, where prototypes are typically imperfect and insignificant parts vary between inputs, the model tends to focus more on capturing significant segments.

#### 5.2 UEA Datasets

We evaluated our model using the UEA multivariate time series repository [2], which contains 30 data sets that span various domains, dimensions, and complexity levels. These datasets show significant variety in their characteristics: the number of classes ranges from 2 to 39, the number of features from 2 to 1345, and the sequence length from 8 to 17984. Each dataset comes with predefined train/test splits. The complete dataset characteristics and corresponding optimal hyperparameters are presented in Table 2 in the Appendix.

We evaluated ProtoTSNet against both explainable and non-explainable methods:

- Ante-hoc explainable: PETSC [14], Shapelet-based method [18] (binary shapelet transform classifier with random shapelet sampling and rotation forest from sktime)
- Post-hoc explainable: XCM [13], MTEX-CNN [1], LITEMVTime [20]
- Non-explainable: ROCKET [9] (state-of-the-art time series classification method), TapNet [39] (established non-explainable prototype-based method)

 $<sup>^2\</sup>mathrm{See}$  https://timeseriesclassification.com

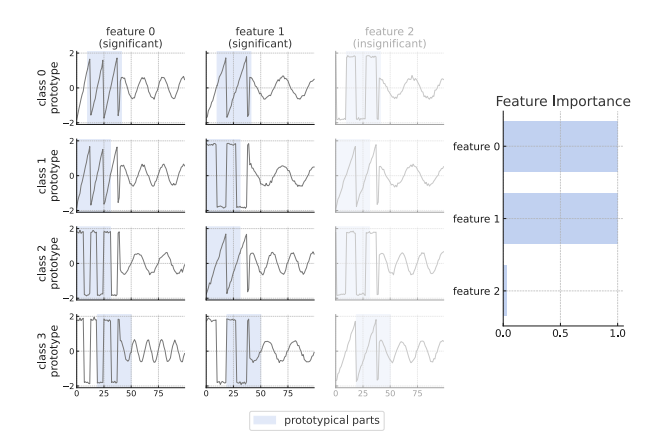


Figure 4: Prototypical parts (blue background) learned on our synthetic dataset and calculated feature importance. Features are split into separate plots for clarity (each row represents a single prototypical part). Each prototype correctly captures the significant part (initial 40 time steps), however, some of them cover the insignificant area as well. This is specific to the design of our model and the experiment setup since capturing a small portion of the significant part is enough to distinguish the classes. There are three features, of which two are significant for the class distinction and one is not. The feature importance calculated reflects this, and the insignificant feature is dimmed out.

We excluded LAXCAT (Table 1) from our comparison due to the lack of clarity regarding the exact preprocessing steps used in the original study, which were crucial to the overall training process. The authors did not include these details in their paper and did not provide a source code implementation.

We conducted all experiments using the original implementations and hyperparameters provided by their respective authors, with exceptions noted for MTEX-CNN (using XCM authors' implementation) and PETSC (modified to use 5-fold cross-validation instead of test set optimization).

For our method, we performed hyperparameter optimization through grid search with 5-fold cross-validation, exploring:

- Reception parameter r: 0.25, 0.5, 0.75, 0.9
- $\bullet$  Prototypical parts length  $L\!\!:\,1\%,\,10\%,\,25\%,\,50\%,\,100\%$  of the time series length

All other hyperparameters remained constant across experiments. Complete cross-validation results are available in our GitHub repository. The model training consisted of two phases:

- Encoder pretraining: 50 epochs as part of an autoencoder with MSE loss
- Main training: four cycles of (joint epochs → prototype projection → last layer optimization), totaling approximately 360 epochs

The classification accuracy scores for all methods are presented in Table 3 in the Appendix, with bold values indicating the best result for each dataset. Incomplete cases are marked as  $\rm "N/A"$  in the table and represent trials that failed

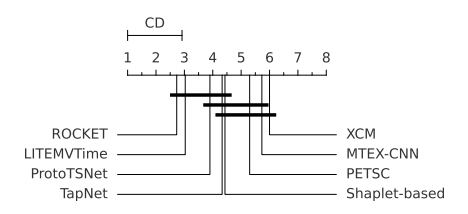


Figure 5: Critical difference diagram for methods evaluated on the UEA multivariate datasets ( $\alpha=0.05$ ). ProtoTSNet achieves competitive performance, ranking best among ante-hoc explainable methods (ProtoTSNet, PETSC, Shapelet-based) and showing comparable performance to non-explainable methods (ROCKET, TapNet) and post-hoc explainable method (LITEMVTime). Note that non-explainable methods and post-hoc explainable methods naturally have accuracy advantages as they are not constrained by ante-hoc explainability requirements.

to complete due to resource constraints being exceeded. Summary statistics, including average ranks and the number of wins/ties, are provided at the bottom of the table. For the purpose of calculating average ranks, we assigned the lowest ranks to the "N/A" cases, as these represent scenarios requiring impractical computational resources.

ProtoTSNet achieves competitive performance across all method categories, ranking best among ante-hoc explainable methods with an average rank of 3.90. Among all methods, ROCKET achieves the best average rank of 2.73, followed by LITEMVTime (3.03). This performance hierarchy reflects the natural accuracy advantages of non-explainable methods and post-hoc explainable methods, which are not constrained by ante-hoc explainability requirements.

Performance analysis reveals dataset-specific patterns. ProtoTSNet demonstrates strong performance on datasets like DuckDuckGeese and HandMovementDirection, where neural network-based methods and ROCKET also perform well, suggesting these datasets benefit from convolutional filtering and temporal pattern extraction capabilities. On datasets like EthanolConcentration and Handwriting, shapelet-based and/or post-hoc methods show superior performance, which may indicate scenarios where global statistical features or fine-grained local patterns are more informative than the intermediate-length prototypical parts learned by our method.

We conducted a statistical analysis of our results using the critical difference test with Nemenyi post-hoc analysis [10]. The resulting critical difference diagram, generated using the Orange data mining library [11] and presented in Figure 5, compares the average ranks across all methods and datasets. In the diagram, methods connected by a horizontal bar do not exhibit statistically significant differences in performance. ProtoTSNet achieves competitive performance among all methods, ranking best among ante-hoc explainable methods and post-hoc explainable methods. Note that non-explainable methods and post-hoc explainable methods naturally have accuracy advantages as they are not constrained by ante-hoc explainability requirements.

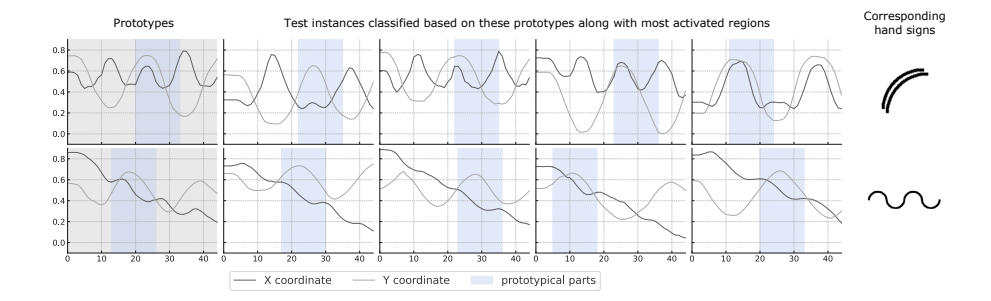


Figure 6: Example prototypes learned on the Libras dataset, along with the instances from the test set that were classified based on these prototypes, and corresponding hand signs from the sign language they represent. The network extracted significant points of the movements, and performs classification based on them. In the first case, the prototype represents a single arch, and it gets recognized correctly regardless of the imperfections of the movement. The second prototype captures a single wave pattern with X coordinate falling below the Y coordinate while moving the hand.

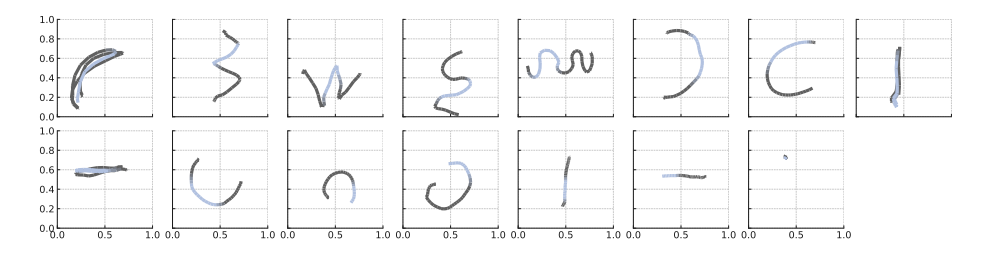


Figure 7: Prototypes for each class of the Libras dataset transformed and presented as 2D hand gestures with prototypical parts shown in blue.

#### 5.2.1 Prototypical Parts

The prototypical parts that demonstrate the interpretability aspect are illustrated using the Libras dataset [12]. The dataset contains data related to hand movement for different signs of the Brazilian Sign Language. It consists of 15 classes of 24 instances each. In Figure 6 we present the learned prototypes for two of the classes, along with instances from the test set that were classified based on these prototypes. In Figure 7 we present prototypes for each class transformed to be presented as 2D hand gestures.

#### 5.3 Ablation Study

To analyze the impact of our architectural choices, we conducted an ablation study comparing four ProtoTSNet variants:

- full variant with grouping encoder and pretraining (GE/P),
- with grouping encoder without pretraining (GE/NP),

- with regular encoder and pretraining (RE/P),
- with regular encoder without pretraining (RE/NP).

All variants used the hyperparameters optimized in previous experiments. The training process consisted of four cycles of (joint epochs  $\rightarrow$  prototype projection  $\rightarrow$  last layer optimization), totaling approximately 360 epochs. When applied, encoder pretraining comprised 50 epochs.

Table 4 included in the Appendix presents the classification accuracy across all datasets. The full variant achieves the best performance among the tested variants with an average rank of 1.90 and 13 wins/ties, followed by the regular encoder without pretraining variant with an average rank of 2.33 and 11 wins/ties.

An interesting observation emerges regarding the impact of pretraining across encoder architectures. Pretraining significantly improves performance with the grouping encoder, but shows a small impact with the regular encoder. This discrepancy may be explained by the pretraining objective: as part of an autoencoder, the encoder learns to represent all features with equal significance. While this might not be optimal for classification, where feature importance varies, the grouping encoder can later selectively disable certain feature groups during ProtoTSNet training thanks to the  $1\times 1$  convolution layer following the encoder.

While the introduction of the grouping encoder initially degrades performance (the non-pretrained grouped encoder ranks last in both average rank and wins/ties), the addition of pretraining not only recovers, but surpasses the regular encoder's performance. The performance varies across datasets: the full variant excels on datasets like Epilepsy and LSST, while the regular encoder performs better on EigenWorms and Handwriting. Some datasets, such as ArticularyWordRecognition, Heartbeat, and JapaneseVowels, show comparable performance across variants.

The critical difference analysis using Friedman test followed by a Nemenyi pairwise post-hoc test for multiple comparisons of mean rank sums [10] presented in Figure 8 compares the average ranks across the four ProtoTSNet variants. The full variant (GE/P) achieves the best average rank of 1.90 and shows a statistically significant improvement over the grouped encoder without pretraining variant (GE/NP).

#### 5.3.1 Parameter Sensitivity Analysis

Our architecture incorporates two key parameters that influence the model behavior:

- prototype length: the length of individual prototypes expressed as a percentage of input time series length,
- reception: the percentage of input features passed to each encoder group, controlling the sparsity of grouping encoder masks.

Figure 9 presents parameter sensitivity analysis across four representative datasets using heatmaps of accuracy across the 2D parameter grid. Additional heatmaps and corresponding bar charts of feature importance for all datasets

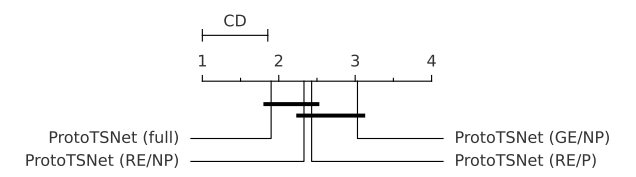


Figure 8: Critical difference diagram for the four ProtoTSNet variants evaluated on the UEA multivariate datasets ( $\alpha=0.05$ ). The full variant (GE/P) shows statistically significant improvement over the grouped encoder without pretraining variant (GE/NP), while other comparisons show no significant differences. Abbreviations used: GE - modified encoder with grouping, RE - regular encoder without grouping, P - encoder pretraining, P - no encoder pretraining. The full variant combines grouping encoder with pretraining.

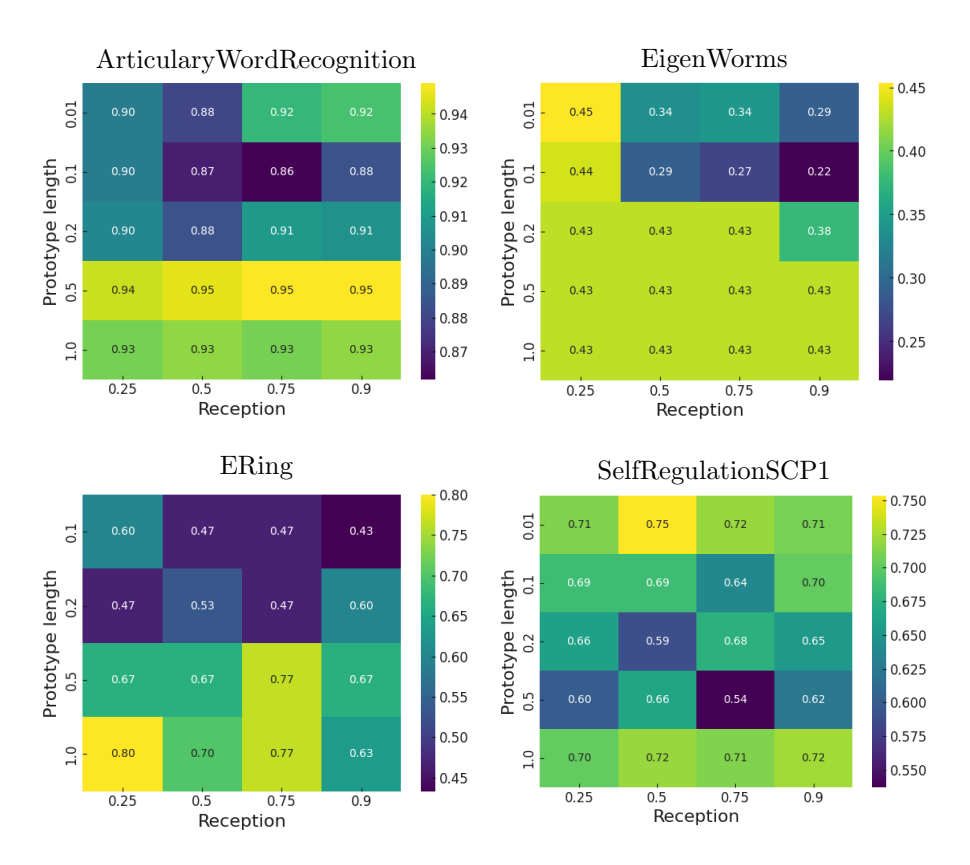


Figure 9: Parameter sensitivity analysis showing classification accuracy across prototype length and reception parameter values for four selected datasets. Heatmaps demonstrate varying sensitivity patterns across different dataset characteristics. Complete analysis with feature importance bar charts for all datasets is provided in Appendix Figure 10.

are provided in Appendix Figure 10. All values represent averages from five cross-validation runs.

The impact of prototype length on classification accuracy varies significantly across datasets. For datasets like ERing and SelfRegulationSCP1 (Figure 9), prototype length substantially influences performance, reflecting the varying lengths of class-characteristic patterns. Some datasets, such as EigenWorms, show good performance with longer prototypes as well, suggesting their ability to capture shorter characteristic patterns. Others, like CharacterTrajectories and SelfRegulationSCP1, exhibit multiple prototype lengths yielding comparable accuracy. This parameter can be effectively tuned using domain expertise, as it corresponds to the expected length of class-distinctive temporal patterns.

The reception parameter's influence on accuracy is generally more subtle and dataset-dependent. While some datasets (Articulary Word Recognition, Ethanol-Concentration) show minimal sensitivity to this parameter, others (LSST, Eigen-Worms) demonstrate more pronounced effects. However, reception strongly influences feature importance calculations, which aligns with its role in controlling feature filtering within the grouping encoder. Higher reception values can lead to overestimated feature importance scores due to increased feature mixing. For practical applications, we recommend initializing this parameter with a high value and gradually reducing it until accuracy begins to degrade (accuracy may initially improve with reduction).

# 6 Summary

In this paper, we presented ProtoTSNet, a novel approach for interpretable multivariate time series classification that provides ante hoc explanations through prototypical parts. Our method addresses a significant gap in the field of explainable time series analysis, where ante hoc approaches for multivariate data are particularly scarce. The key advantages of our approach include the ability to identify significant temporal patterns through prototypes, calculate feature importance, and provide explanations that are accessible to domain experts without requiring a deep understanding of the underlying algorithms.

Our evaluation on the UEA multivariate time series archive demonstrates that ProtoTSNet achieves the best performance among ante-hoc explainable methods, followed by the shapelet-based approach, which despite its interpretability relies on rotation forests that may complicate direct explanation understanding. While some methods such as ROCKET (non-explainable) and LITEMVTime (post-hoc explainable) achieve higher average ranks, ProtoT-SNet maintains competitive performance while providing the advantage of direct ante-hoc interpretability. Through ablation studies, we validated our architectural choices and provided insights into parameter selection through sensitivity analysis. Statistical analysis using critical difference diagrams confirms the significance of our results.

The prototype-based nature of our explanations offers direct interpretability through the "this resembles that" principle, providing clearer explanations than methods that rely on ensemble techniques or complex feature transformations. This opens up interesting possibilities for integration with symbolic approaches, potentially bridging the gap between neural and symbolic representations in time series analysis. Our future work will focus on domain-specific

applications and user studies to evaluate the intuitiveness of the model's explanations, enhancing our understanding of the model's capabilities and limitations in practical contexts.

# References

- [1] Roy Assaf, Ioana Giurgiu, Frank Bagehorn, and Anika Schumann. MTEX-CNN: Multivariate Time Series EXplanations for Predictions with Convolutional Neural Networks. In 2019 IEEE International Conference on Data Mining (ICDM), pages 952–957, 2019.
- [2] Anthony Bagnall, Hoang Anh Dau, Jason Lines, Michael Flynn, James Large, Aaron Bostrom, Paul Southam, and Eamonn Keogh. The UEA multivariate time series classification archive, 2018. arXiv preprint arXiv:1811.00075, 2018.
- [3] Paul Boniol, Mohammed Meftah, Emmanuel Remy, and Themis Palpanas. dCAM: Dimension-wise class activation map for explaining multivariate data series classification. In *Proceedings of the 2022 International Conference on Management of Data*, pages 1175–1189, 2022.
- [4] Nestor Cabello, Elham Naghizade, Jianzhong Qi, and Lars Kulik. Fast, accurate and explainable time series classification through randomization. Data Mining and Knowledge Discovery, 38(2):748–811, 2024.
- [5] Nestor Cabello, Elham Naghizade, Jianzhong Qi, and Lars Kulik. Fast, accurate and explainable time series classification through randomization. *Data Mining and Knowledge Discovery*, 38(2):748–811, 2024.
- [6] Chaofan Chen, Oscar Li, Daniel Tao, Alina Barnett, Cynthia Rudin, and Jonathan K Su. This looks like that: deep learning for interpretable image recognition. Advances in neural information processing systems, 32, 2019.
- [7] DARPA. Explainable Artificial Intelligence. URL https://www.darpa.mil/program/explainable-artificial-intelligence.
- [8] Subhajit Das, Panpan Xu, Zeng Dai, Alex Endert, and Liu Ren. Interpreting deep neural networks through prototype factorization. In 2020 International Conference on Data Mining Workshops (ICDMW), pages 448–457. IEEE, 2020.
- [9] Angus Dempster, François Petitjean, and Geoffrey I Webb. ROCKET: exceptionally fast and accurate time series classification using random convolutional kernels. *Data Mining and Knowledge Discovery*, 34(5):1454–1495, 2020
- [10] Janez Demšar. Statistical comparisons of classifiers over multiple data sets. J. Mach. Learn. Res., 7:1–30, December 2006. ISSN 1532-4435.
- [11] Janez Demšar, Tomaž Curk, Aleš Erjavec, Črt Gorup, Tomaž Hočevar, Mitar Milutinovič, Martin Možina, Matija Polajnar, Marko Toplak, Anže Starič, Miha Štajdohar, Lan Umek, Lan Žagar, Jure Žbontar, Marinka Žitnik, and Blaž Zupan. Orange: Data mining toolbox in python. Journal of Machine Learning Research, 14:2349–2353, 2013.

- [12] Daniel B Dias, Renata CB Madeo, Thiago Rocha, Helton H Biscaro, and Sarajane M Peres. Hand movement recognition for brazilian sign language: a study using distance-based neural networks. In 2009 international joint conference on neural networks, pages 697–704. IEEE, 2009.
- [13] Kevin Fauvel, Tao Lin, Véronique Masson, Élisa Fromont, and Alexandre Termier. XCM: An explainable convolutional neural network for multivariate time series classification. *Mathematics*, 9(23):3137, 2021.
- [14] Len Feremans, Boris Cule, and Bart Goethals. PETSC: pattern-based embedding for time series classification. *Data Mining and Knowledge Discovery*, 36(3):1015–1061, 2022.
- [15] Alan H Gee, Diego Garcia-Olano, Joydeep Ghosh, and David Paydarfar. Explaining deep classification of time-series data with learned prototypes. In CEUR workshop proceedings, volume 2429, page 15. NIH Public Access, 2019.
- [16] Bryce Goodman and Seth Flaxman. EU regulations on algorithmic decision-making and a "right to explanation", 2016. Comment: presented at 2016 ICML Workshop on Human Interpretability in Machine Learning (WHI 2016), New York, NY.
- [17] Philipp Hacker and Jan-Hendrik Passoth. Varieties of AI Explanations Under the Law. From the GDPR to the AIA, and Beyond, pages 343–373. Springer International Publishing, Cham, 2022.
- [18] Jon Hills, Jason Lines, Edgaras Baranauskas, James Mapp, and Anthony Bagnall. Classification of time series by shapelet transformation. *Data Min. Knowl. Discov.*, 28(4):851–881, July 2014. ISSN 1384-5810.
- [19] Tsung-Yu Hsieh, Suhang Wang, Yiwei Sun, and Vasant Honavar. Explainable multivariate time series classification: a deep neural network which learns to attend to important variables as well as time intervals. In Proceedings of the 14th ACM international conference on web search and data mining, pages 607–615, 2021.
- [20] Ali Ismail-Fawaz, Maxime Devanne, Stefano Berretti, Jonathan Weber, and Germain Forestier. Look into the lite in deep learning for time series classification, 2025.
- [21] Sayash Kapoor and Arvind Narayanan. Leakage and the reproducibility crisis in machine-learning-based science. *Patterns*, August 2023. ISSN 2666-3899. Publisher: Elsevier.
- [22] Shruti Kaushik, Abhinav Choudhury, Pankaj Kumar Sheron, Nataraj Dasgupta, Sayee Natarajan, Larry A Pickett, and Varun Dutt. AI in healthcare: time-series forecasting using statistical, neural, and ensemble architectures. Frontiers in big data, 3:4, 2020.
- [23] Aurelien Teguede Keleko, Bernard Kamsu-Foguem, Raymond Houe Ngouna, and Amèvi Tongne. Artificial intelligence and real-time predictive maintenance in industry 4.0: a bibliometric analysis. *AI and Ethics*, 2 (4):553–577, 2022.

- [24] Thach Le Nguyen, Severin Gsponer, Iulia Ilie, Martin O'reilly, and Georgiana Ifrim. Interpretable time series classification using linear models and multi-resolution multi-domain symbolic representations. *Data mining and knowledge discovery*, 33:1183–1222, 2019.
- [25] Oscar Li, Hao Liu, Chaofan Chen, and Cynthia Rudin. Deep learning for case-based reasoning through prototypes: A neural network that explains its predictions. In *Proceedings of the AAAI Conference on Artificial Intel*ligence, volume 32, 2018.
- [26] Jessica Lin, Eamonn Keogh, Stefano Lonardi, and Bill Chiu. A symbolic representation of time series, with implications for streaming algorithms. In Proceedings of the 8th ACM SIGMOD Workshop on Research Issues in Data Mining and Knowledge Discovery, DMKD '03, page 2–11, New York, NY, USA, 2003. Association for Computing Machinery. ISBN 9781450374224.
- [27] Scott M. Lundberg and Su-In Lee. A unified approach to interpreting model predictions. In *Proceedings of the 31st International Conference on Neural Information Processing Systems*, NIPS'17, page 4768–4777, Red Hook, NY, USA, 2017. Curran Associates Inc. ISBN 9781510860964.
- [28] Matthew Middlehurst, Patrick Schäfer, and Anthony Bagnall. Bake off redux: a review and experimental evaluation of recent time series classification algorithms. arXiv preprint arXiv:2304.13029, 2023.
- [29] Yao Ming, Panpan Xu, Huamin Qu, and Liu Ren. Interpretable and steerable sequence learning via prototypes. In *Proceedings of the 25th ACM SIGKDD International Conference on Knowledge Discovery & Data Mining*, pages 903–913, 2019.
- [30] Rami Mochaourab, Arun Venkitaraman, Isak Samsten, Panagiotis Papapetrou, and Cristian R Rojas. Post hoc explainability for time series classification: Toward a signal processing perspective. *IEEE signal processing* magazine, 39(4):119–129, 2022.
- [31] Sebastian Müller, Vanessa Toborek, Katharina Beckh, Matthias Jakobs, Christian Bauckhage, and Pascal Welke. An empirical evaluation of the rashomon effect in explainable machine learning. In Danai Koutra, Claudia Plant, Manuel Gomez Rodriguez, Elena Baralis, and Francesco Bonchi, editors, *Machine Learning and Knowledge Discovery in Databases: Research Track*, pages 462–478, Cham, 2023. Springer Nature Switzerland.
- [32] Antonin Poché, Lucas Hervier, and Mohamed-Chafik Bakkay. Natural example-based explainability: A survey. In Luca Longo, editor, *Explainable Artificial Intelligence*, pages 24–47, Cham, 2023. Springer Nature Switzerland. ISBN 978-3-031-44067-0.
- [33] Marco Tulio Ribeiro, Sameer Singh, and Carlos Guestrin. "Why Should I Trust You?": Explaining the Predictions of Any Classifier. In Proceedings of the 22nd ACM SIGKDD International Conference on Knowledge Discovery and Data Mining, KDD '16, page 1135–1144, New York, NY, USA, 2016. Association for Computing Machinery. ISBN 9781450342322.

- [34] Zohaib Salahuddin, Henry C. Woodruff, Avishek Chatterjee, and Philippe Lambin. Transparency of deep neural networks for medical image analysis: A review of interpretability methods. *Computers in Biology and Medicine*, 140:105111, 2022. ISSN 0010-4825. URL https://www.sciencedirect.com/science/article/pii/S0010482521009057.
- [35] Ramprasaath R Selvaraju, Michael Cogswell, Abhishek Das, Ramakrishna Vedantam, Devi Parikh, and Dhruv Batra. Grad-CAM: visual explanations from deep networks via gradient-based localization. *International journal of computer vision*, 128:336–359, 2020.
- [36] Omer Berat Sezer, Mehmet Ugur Gudelek, and Ahmet Murat Ozbayoglu. Financial time series forecasting with deep learning: A systematic literature review: 2005–2019. Applied soft computing, 90:106181, 2020.
- [37] Wensi Tang, Lu Liu, and Guodong Long. Interpretable time-series classification on few-shot samples. In 2020 International Joint Conference on Neural Networks (IJCNN), pages 1–8. IEEE, 2020.
- [38] Andreas Theissler, Francesco Spinnato, Udo Schlegel, and Riccardo Guidotti. Explainable AI for time series classification: a review, taxonomy and research directions. *IEEE Access*, 2022.
- [39] Xuchao Zhang, Yifeng Gao, Jessica Lin, and Chang-Tien Lu. Tapnet: Multivariate time series classification with attentional prototypical network. In Proceedings of the AAAI Conference on Artificial Intelligence, volume 34, pages 6845–6852, 2020.

# Appendix A Datasets quantitative description and results

Table 2: UEA multivariate datasets characteristics together with the hyperparameters found through a 5-fold cross-validation. Train stands for the training set size, test for the test set size, r stands for reception of the encoder and L

stands for prototype length as a fraction of time series length.

Dataset Dataset	Train	Test	Dims	Len	Classes	r	L
ArticularyWordRecognition	275	300	9	144	25	0.75	0.5
AtrialFibrillation	15	15	2	640	3	0.5	0.2
BasicMotions	40	40	6	100	4	0.25	0.2
CharacterTrajectories	1422	1436	3	182	20	0.9	1
Cricket	108	72	6	1197	12	0.75	0.1
DuckDuckGeese	50	50	1345	270	5	0.5	0.01
ERing	30	270	4	65	6	0.25	1
EigenWorms	128	131	6	17984	5	0.25	0.01
Epilepsy	137	138	3	206	4	0.5	1
EthanolConcentration	261	263	3	1751	4	0.25	0.01
FaceDetection	5890	3524	144	62	2	0.9	1
FingerMovements	316	100	28	50	2	0.5	1
HandMovementDirection	160	74	10	400	4	0.5	1
Handwriting	150	850	3	152	26	0.75	0.5
Heartbeat	204	205	61	405	2	0.5	1
InsectWingbeat	30000	20000	200	30	10	0.25	0.1
JapaneseVowels	270	370	12	29	9	0.5	1
LSST	2459	2466	6	36	14	0.75	0.1
Libras	180	180	2	45	15	0.9	0.5
MotorImagery	278	100	64	3000	2	0.5	0.01
NATOPS	180	180	24	51	6	0.5	0.5
PEMS-SF	267	173	963	144	7	0.75	1
PenDigits	7494	3498	2	8	10	0.75	0.5
PhonemeSpectra	3315	3353	11	217	39	0.75	0.1
RacketSports	151	152	6	30	4	0.9	0.1
SelfRegulationSCP1	268	293	6	896	2	0.5	0.01
SelfRegulationSCP2	200	180	7	1152	2	0.5	0.2
SpokenArabicDigits	6599	2199	13	93	10	0.75	1
StandWalkJump	12	15	4	2500	3	0.75	0.5
UWaveGestureLibrary	120	320	3	315	8	0.75	0.5

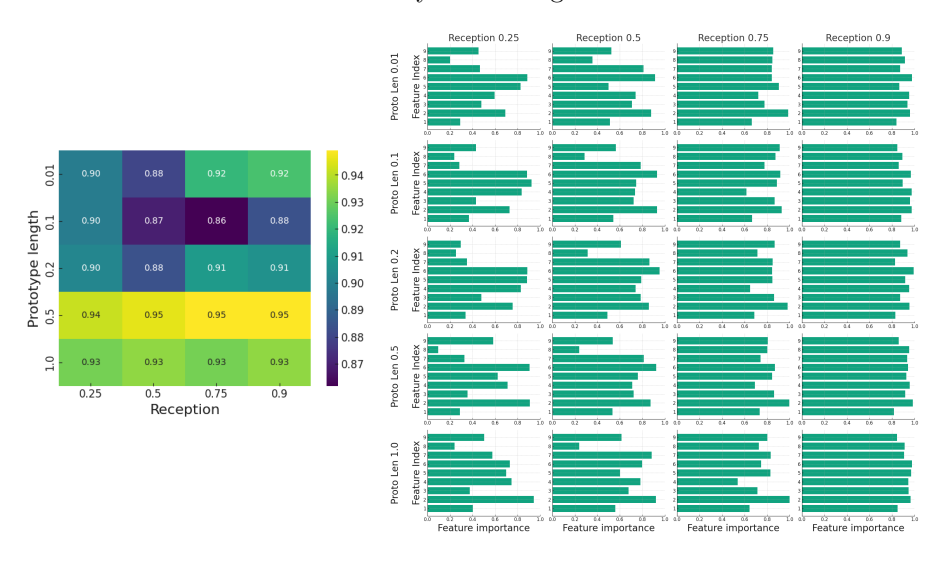
Table 3: Accuracy scores achieved by the methods we tested on the UEA multivariate datasets. Best results in **bold**. Abbreviations for methods: PTS - ProtoTSNet, PET - PETSC, Sha - Shaplet-based, MTC - MTEX-CNN, Lite - LITEMVTime, Tap - TapNet, ROC - ROCKET.

D. 4. 4	ante hoc			post hoc			non-explainable	
Dataset	PTS	PET	Sha	XCM	MTC	Lite	Tap	ROC
ArticularyWordRecognition	96.7	99.3	97.0	72.9	94.2	98.7	98.3	99.3
AtrialFibrillation	33.3	30.7	32.0	30.7	33.3	21.3	25.3	6.7
BasicMotions	100.0	94.5	94.5	95.5	97.0	100.0	100.0	100.0
CharacterTrajectories	98.1	93.3	97.6	95.7	95.8	99.6	99.7	N/A
Cricket	94.4	99.4	97.2	71.7	89.4	98.6	97.8	100.0
DuckDuckGeese	68.8	42.0	43.6	31.6	51.2	N/A	48.8	52.0
EigenWorms	38.9	N/A	N/A	28.2	42.0	68.9	47.8	90.8
Epilepsy	96.8	98.4	98.8	89.7	92.8	99.6	97.0	99.3
ERing	82.2	88.3	92.5	20.6	84.5	93.1	82.0	98.5
EthanolConcentration	29.4	50.6	75.7	28.8	28.5	26.3	28.0	44.5
FaceDetection	63.3	56.2	N/A	55.5	50.0	65.0	51.3	64.4
FingerMovements	53.8	52.6	55.8	51.4	49.0	62.8	49.6	54.0
HandMovementDirection	53.0	25.9	49.5	32.4	36.5	40.3	35.9	51.4
Handwriting	20.2	40.2	40.6	17.6	21.5	64.1	53.0	59.5
Heartbeat	72.0	67.4	72.0	71.8	66.3	67.4	73.6	74.6
InsectWingbeat	64.9	N/A	N/A	61.2	69.5	73.5	47.2	N/A
JapaneseVowels	97.2	N/A	87.8	94.1	93.5	98.9	98.1	N/A
Libras	90.1	81.6	87.9	59.1	64.6	92.1	85.4	90.0
LSST	60.2	54.1	64.1	56.7	40.8	31.3	46.8	63.7
MotorImagery	52.8	N/A	51.2	54.0	50.0	51.0	48.6	58.0
NATOPS	94.8	83.0	85.7	83.4	89.0	95.9	96.4	88.9
PEMS-SF	84.9	91.3	95.6	69.4	49.5	71.9	76.6	83.2
PenDigits	97.0	86.7	N/A	95.7	89.4	98.6	97.1	98.3
PhonemeSpectra	23.9	24.3	N/A	10.5	6.2	31.1	9.2	27.6
RacketSports	83.4	83.2	83.0	66.3	69.5	86.7	84.3	89.5
SelfRegulationSCP1	76.0	69.7	83.7	68.3	67.6	80.2	65.8	84.3
SelfRegulationSCP2	50.9	49.4	52.0	52.6	50.0	53.4	54.3	57.2
SpokenArabicDigits	94.0	N/A	67.0	97.6	97.2	99.6	98.4	N/A
StandWalkJump	34.7	37.8	50.7	24.0	42.7	44.0	26.7	53.3
UWaveGestureLibrary	84.1	88.8	88.1	81.4	82.6	91.4	91.9	94.1
Avg. Rank	3.90	5.30	4.43	6.00	5.73	3.03	4.33	2.73
Wins/Ties	3	0	3	0	1	11	3	12

Table 4: Classification accuracy scores for four ProtoTSNet variants on UEA multivariate datasets. Best results are shown in **bold**. Variant naming convention: GE - grouping encoder, RE - regular encoder, P - with pretraining, NP - without pretraining. The full variant (GE/P) combines grouping encoder with pretraining.

Dataset	GE/P	GE/NP	RE/P	RE/NP	
ArticularyWordRecognition	96.7	96.5	96.5	96.8	
AtrialFibrillation	33.3	36.0	26.7	33.3	
BasicMotions	100.0	100.0	100.0	100.0	
CharacterTrajectories	98.1	97.9	97.9	97.8	
Cricket	94.4	91.4	94.7	92.5	
DuckDuckGeese	68.8	62.8	68.0	64.4	
EigenWorms	38.9	32.2	28.9	57.7	
Epilepsy	96.8	87.7	88.1	80.0	
ERing	82.2	80.3	78.8	82.0	
EthanolConcentration	29.4	28.7	29.4	28.6	
FaceDetection	63.3	59.9	61.1	60.9	
FingerMovements	53.8	52.0	51.0	52.0	
HandMovementDirection	53.0	50.8	53.8	42.2	
Handwriting	20.2	19.4	20.8	25.0	
Heartbeat	72.0	72.2	71.7	71.8	
InsectWingbeat	64.9	63.1	65.4	64.8	
JapaneseVowels	97.2	96.8	97.6	97.2	
Libras	90.1	88.6	90.0	87.6	
LSST	60.2	53.1	55.9	56.9	
MotorImagery	52.8	50.6	51.6	53.8	
NATOPS	94.8	94.7	94.9	96.4	
PEMS-SF	84.9	86.9	86.8	85.8	
PenDigits	97.0	96.7	98.6	98.6	
PhonemeSpectra	23.9	21.7	23.7	24.0	
RacketSports	83.4	83.8	85.5	85.8	
SelfRegulationSCP1	76.0	73.8	75.0	72.5	
SelfRegulationSCP2	50.9	50.4	48.2	52.6	
SpokenArabicDigits	94.0	96.5	96.2	97.3	
StandWalkJump	34.7	33.3	28.0	34.7	
UWaveGestureLibrary	84.1	82.8	83.2	80.7	
Avg. Rank	1.90	3.03	2.43	2.33	
Wins/Ties	13	4	6	11	

# ${\bf Articulary Word Recognition}$



# ${\bf Character Trajectories}$

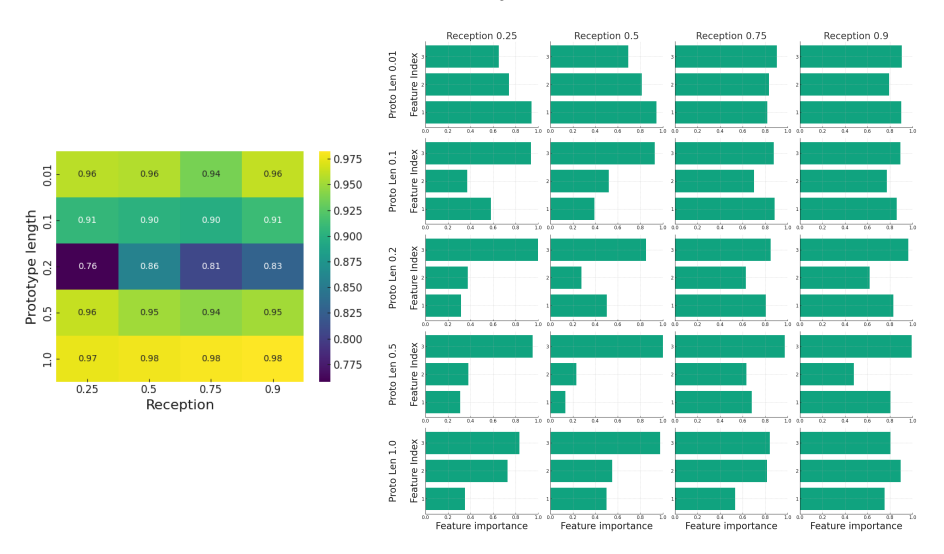
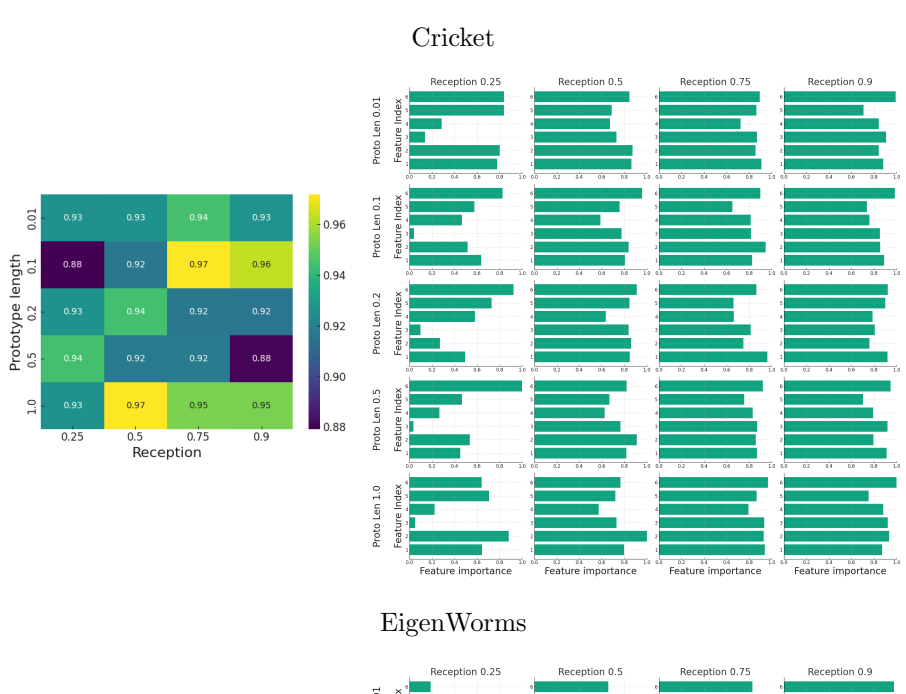


Figure 10: Parameter sensitivity analysis for selected datasets, examining prototype length and reception parameters. Left: Heatmaps showing average classification accuracy across the parameter grid. Right: Bar charts showing average feature importance scores across the same parameter combinations. The parameter grid explores five prototype lengths (as fractions of input time series length) and four reception values (controlling feature sparsity in the grouping encoder). All values are averaged over five cross-validation runs.



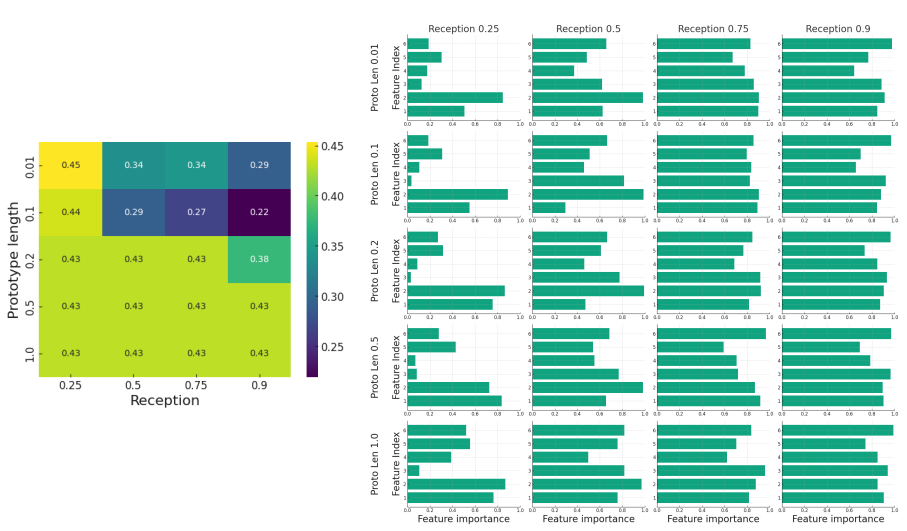
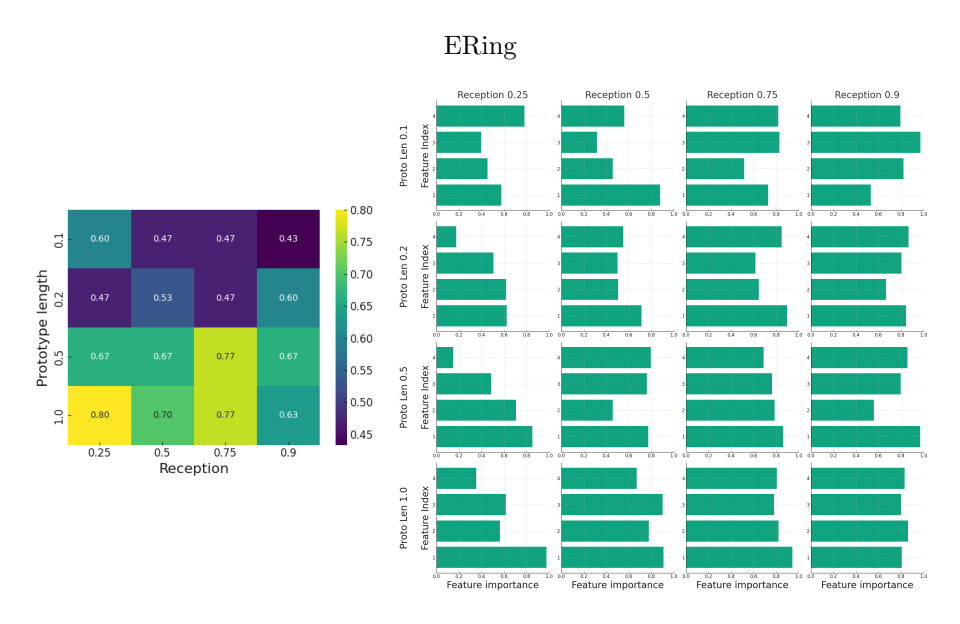


Figure 10: (contd)



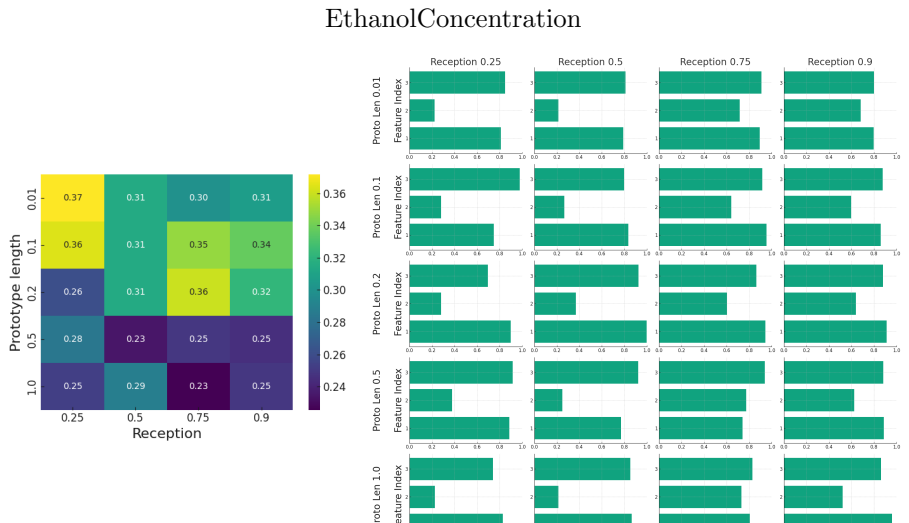
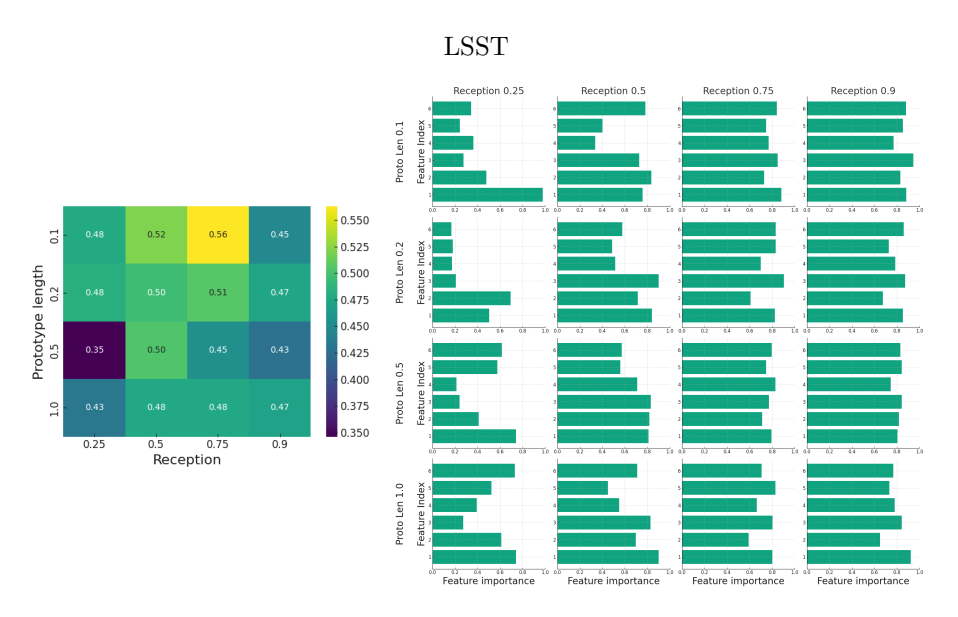


Figure 10: (contd)

Feature importance

Feature importance



# ${\bf SelfRegulation SCP1}$

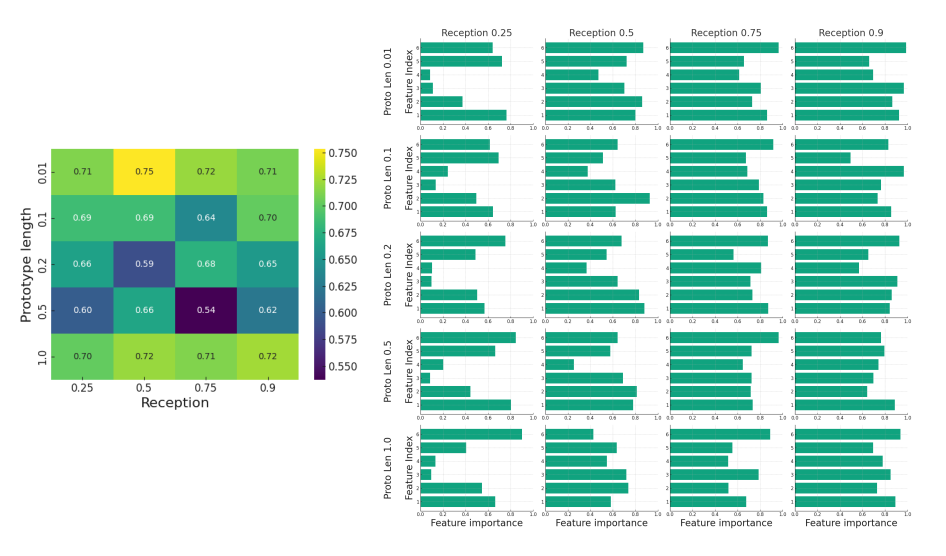


Figure 10: (contd)